

Turbulent Flow Simulation over Two- Dimensional Simplified Car in Dusty Fluid Medium

Sujit Mishra, Ashok Misra*

Centurion University of Technology and Management, Odisha, India

*Corresponding Author: Ashok Misra

Abstract

Automotive aerodynamic studies are typically conducted on simplified car models in order to examine flow patterns and their effect on drag forces. Simulations using Computational Fluid Dynamics (CFD) provides an effective tool to simulate these flow parameters that highly dependent on the quality of the turbulence model used. This paper focuses to investigate the drag performance and overall flow characteristics in dusty fluid environment using k - ϵ turbulence scheme considering two dimensional 25° rear slant Ahmed body. Results are compared with the existing experimental and single phase turbulence models. In presence of suspended dust particles in air, it is observed that the overall drag coefficient gets attenuates leading towards more precise values to that of existing experimental results.

Keywords: Simplified car, Turbulence Models, Ahmed Body, Aerodynamics, Dusty fluid

1. Introduction

External aerodynamics has a significant effect on a number of essential components of an automobile, including the vehicle's stability, level of comfort, and amount of gasoline consumed while traveling at highway speeds. The road test gets more difficult, despite the fact that it is one of the most effective methods for investigating external aerodynamics. That's why, in order to conduct aerodynamics studies, the reversibility principle of motion is used, which states that "the force acting on a body when a fluid flows around it at constant velocity is equivalent to the force experienced by a body in uniform and translatory motion in a stationary atmosphere." Whilst wind tunnel testing is still commonly employed, the development of useful numerical tools is expanding as the cost of numerical simulations continues to decrease. However, the fundamental challenge is that the automotive industry and industrial applications are currently experiencing in a lack of robust and accurate computational fluid dynamics (CFD) methodologies. External flows with a large Reynolds number exhibit extremely turbulent behaviour in addition to three-dimensional separation and reattachment phenomena. The capacity of a CFD simulation to effectively simulate these flow parameters is highly dependent on the quality of the turbulence model used.

Throughout the decades, the use of reference automobile models (Le Good and Garry, 2004) have served

the role of giving designers insight into the basic generic flow architecture of a vehicle. Because there have been so many studies of individual automobile models, almost all of them use a simplified or general car model because of the following two key reasons. While generic models focus on the influence of a particular geometric feature, the insights collected through these models are more fundamental and universal since they focus on the basics of how any geometric effect operates. A second benefit of using a generic benchmark model is that it allows researchers to interact and collaborate more readily, which will enable them to make future breakthroughs. Due to these advantages, reference car models are frequently used to study several elements of automotive aerodynamics, such as flow characterisation, ground simulation, drag reduction, flow control, acoustic performance, and ventilation design.

The most well-known universal simplified model developed (S. R. Ahmed, 1984) known as Ahmed model has been focused in most of the studies because of its simplified geometry to replicate some of the bulk key flow features around a realistic car model – especially the rear end. The results shows almost 85% of body drag is the pressure drag generated towards the rear end of the body and the wake flow is exhibited in the form of vortices depending upon the slant angle. (Fares, 2006) has predicted the capability and feasibility in lattice Boltzmann solver taking a very large eddy simulation (VLES) framework over the 25° slant Ahmed model but found difficulties in attaining the time steps that required for the flow parameters towards converging. (Guilmineau, 2008) has proposed a CFD simulation technique called as a quadratic explicit algebraic stress model (EASM) that has been applied to the Ahmed body with 25° and 35° slant angles. In both cases, the scheme could predict 3% less values of the drag than that of the other scheme results. Further, it has been found that all the simulations scheme used in the study with a massive flow separation particularly at 25° slant body posing a strong challenge towards the establishing of turbulence schemes. (Morgut and Nobile, 2012) has done and emphasis on the influence of two turbulence schemes such as Shear Stress Transport (SST) and Baseline-Reynolds Stress Model (BSL) used over hexa-structured meshes with hybrid- unstructured meshes around the marine propellers. There is a slightly better prediction of flow fields in the BSL scheme than the SST turbulence model. (Serre et al., 2013) has investigated two different eddy- resolving modelling approaches, i.e. Large Eddy

Simulations (LES) and Detached Eddy Simulation (DES) schemes around the 25° slant Ahmed body. In their work, they reveal out the issues arises for the computational cost and ease implementation in their schemes without effecting the quality of results. Similar studies from (Aljure et al., 2014) has been presented a comparative study about the flows and turbulent structures through LES modelling with two various types of simplified models. (Tientcheu-Nsiewe et al., 2016; Mishra et al., 2017) investigates for the Reynolds Averaged Navier–Stokes (RANS) equations over the Ahmed model taking second order upwind scheme to get the results of different flow parameters viz. drag force, drag coefficient, turbulent kinetic energy, and wake flow structures. Moreover, using a hybrid RANS-LES model from (Ashton et al., 2016) benefits than the RANS models in terms of the force coefficients, and general flow field for the Ahmed car body. It is worth noting that nearly all of the aforementioned studies given emphasis on the reliability and accuracy of the numerical turbulence techniques for simulating external flow phenomena in a single phase fluid medium specifically clean air. But in reality, ambient air, used for the aerodynamic experiments in wind tunnel setups, is not only the clear air, but it comprises of air with suspended particles. Considering the air with suspended particles is not a new concept in CFD analysis but it's indeed a new to handle external aerodynamics studies. Moreover, some analysis done from the recent works from (Gaylard et al., 2017) uses very large eddy simulation (VLES) scheme showing the water sprayed particle effects and its deposition pattern in the wakes regions. Also a similar study, from (Mishra et al., 2019) that contains air and sand particles flows over the 2D Ahmed model used for the investigation of the aerodynamic flow parameters. In their investigation, un-steady RANS (URANS) mixture scheme shows a rise in the in drag coefficient, turbulent kinetic energy which has occurred because of high sand volume fraction levels.

Thus, taking into account all research gaps, the present analysis adopts a k-epsilon turbulent scheme in 2D Ahmed computational domain to investigate the drag performance and overall flow characteristics in the presence of a dusty fluid environment. Dusty fluids are a two-phase Eulerian treatment based models in which the granular secondary phase interacts with primary phase fluid air. The purpose is to find the effects of aerodynamic parameters such as drag coefficients, flow features in the wakes region on the 25° slanted Ahmed body when the dusty fluid concentrations set to 0.1% using flow solver ANSYS Fluent v19.

2. Geometry Specification

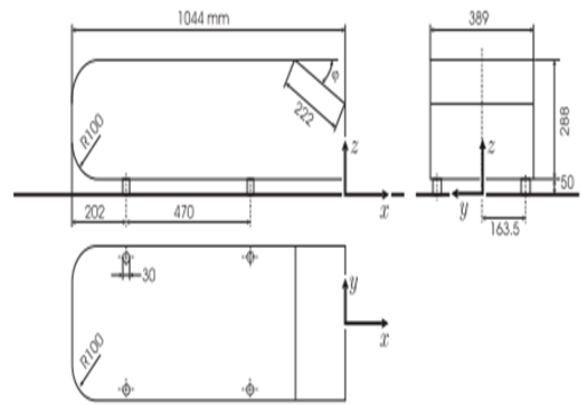


Figure 1. Two Dimensional Geometry specification of Ahmed Body.

The Ahmed model (S. R. Ahmed, 1984) used for the numerical simulations is shown in Fig. 1. Most of the drag of this body is because of the pressure drag, which is generated at the rear end. The structure of the wake is very complex, with a separation zone and counter-rotating vortices generated at the slant side edges. The strength of the separation is determined by the slant angle. For the present case, the rear slant angle kept at 25°, as a result, the flow gets separates in the upstream end of the slant surface which again reattaches in the downstream that has been observed in the experiments (Lienhart and Becker, 2003). The Ahmed Body” comprises the length $L=1044\text{mm}$, and the height $H=288\text{mm}$. The front nose dimensions were fixed with a radius of 100mm and slant length of 222mm, respectively.

3. Computational Domain

For the present analysis, a 2D computational domain has been set to perform the simulations. The computational domain as a rectangular box made in Ansys fluent as shown in figure 2, represents the fluid with suspended particles past over the Ahmed body model. The reference axis (X, Y, Z), point O as shown in Figure 1, is linked to the model and is kept with ground clearance $G=50\text{mm}$. The Reynolds number $Re=7.68 \times 10^5$, calculated based on the height of the geometry model with the incoming velocity, $U_\infty=40\text{ m/s}$ respectively. The value for the Reynolds number is the same as that being used in the wind tunnel experiments (Lienhart and Becker, 2003) which were conducted in a $3/4$ open test section with the blockage ratio of 4%. The computational domain for Ahmed Body specifications has been listed in Table 1.

Table 1. Computational Domain Specifications for Ahmed Body

Model	Parameter
Dimension	2D
Length of Ahmed Body	1.044 m
Height of Ahmed Body	0.288 m
Rear Slant Angle	25 Deg
Total Length of Computational Domain	7m

Total Height of the Computational Domain	3m
Ground Clearance	0.05m
Reynolds Number	7.68×10^5 , based on height

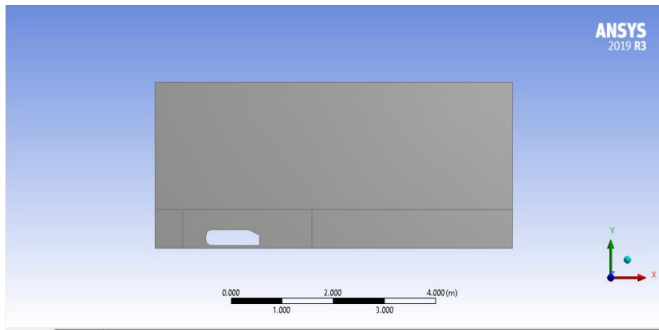


Figure 2. Computational Domain for 2D Ahmed Body

As the present analysis is done over a 2D computational domain, the boundary conditions have been implemented with the edges. At the outlet edge in the computational domain set to atmospheric pressure outlet conditions. The rest edges of the geometry have been given with walls with the no-slip condition. The values for the turbulent intensity are limited to 1% based on the experiments and simulations.(S. R. Ahmed, 1984; Khan and Umale, 2014).

4. Meshing

The computational domain presented in the previous step gets discretized with unstructured 2D triangular elements using the meshing module available in Ansys Fluent workbench. The patch conforming meshing technique provides the simplest approach to discretize the domain. Four types of meshing such as coarse, medium, fine, and ultra-fine mesh set with maximum element sizes as 30mm, 15mm, 7.5mm, and 2mm respectively to conduct the grid independence test.

Table 2. Setup Details for the Meshing

Meshing	Type/Parameters
Element Type	Triangles with Hexa
First Layer Thickness	0.0002 m
Maximum Layers	6
Growth Rate	1.2

Further to capture all details in the boundary layer flow phenomenon, refinement of grids near the walls of the Ahmed body with prism layers that have been fixed with a

Y^+ of 30 with wall function, maximum of 6 layers that gradually increasing with a rate of 1.2 has been provided. Table 2 shows the meshing setup.

5. Grid Independent Test

Mesh convergence study or grid independence study is the way to find an optimum grid size for the present simulated problem, which shows that after this size the solution won't be affected by irrespective of increasing grid size. Table 3, shows a comparison between the overall elements generated in the different grid systems with the coefficient of drag values. The plot between the Drag Coefficient (Cd) and the Number of elements generated at various meshing is shown in Figure 3. A similar approach has been adopted for the grid independency test (Pandey et al. 2021). It can be clearly understood that with increasing the total amount of grid elements, the drag coefficients levels up at the particular amount of grid elements.

Table 3. Comparison for different mesh elements with the obtain drag coefficient values

Mesh No	Mesh Element Size	No. of Elements	Cd
Mesh 1	30 mm	65382	0.334
Mesh 2	15 mm	202130	0.328
Mesh 3	7.5 mm	776323	0.312
Mesh 4	5 mm	1086521	0.310

6. Validation Test

A two-phase URANS Realizable k-ε turbulence setup for the validating process in the present simulation approach uses the concept of phasic volume fractions where the volume fractions in the secondary dusty fluid medium taken as insignificant amount such that the relative density in simulations generates a similar and equivalent effect used in previous studies (Guilmineau et al. 2018)that gets matches with the existing single-phase simulations. Comparing the drag coefficients, the grid independence is achieved with the fine level mesh. Therefore, the mesh is set as the baseline considerations for all further analyses. Table 4 represents a comparison for two-phase URANS Realizable k-ε turbulence with existing results of single-phase URANS Realizable k-ε turbulence models. It can be observed that the drag coefficient values in the present simulation analysis make good attainment at the same level of accuracy and hence validates the simulation procedure.

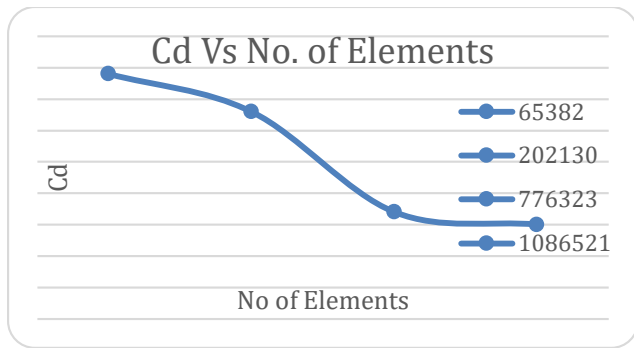


Figure 3. Mesh independency test for 2D Ahmed Body

Table 4. Validation of Numerical Simulation Approach with existing Single phase simulations

Study	Turbulent Model	Drag coefficient
(Khan and Umale, 2014)	Standard k-ε	0.310
(Guilmineau et al. 2018)	SST-k-ω	0.307
Present study	Realizable k-ε	0.312

7. Governing Equations of Flow Field in Dusty Fluid Medium

The mathematical modeling of the two-phase turbulence flow field are described below. These governing equations of flow field are used in ANSYS Fluent v19 (Fluent Guide) by considering the primary phase as air medium and the secondary phase as suspended dust particulate medium.

The volume of phase q , V_q is defined by

$$V_q = \int_V \alpha_q dV,$$

$$\text{where} \quad \sum_{q=1}^n \alpha_q = 1 \quad (1)$$

and the effective density of phase q is

$$\hat{\rho}_q = \alpha_q \rho_q \quad (2)$$

where, ρ_q is the physical density of phase q and α_q is the phasic volume fractions of the multiphase flow.

Equation of Continuity for q^{th} Phase

The volume fraction of q^{th} phase is calculated from a continuity equation:

$$\frac{1}{\rho_{rq}} \left(\frac{\partial}{\partial t} (\alpha_q \rho_q) + \nabla \cdot (\alpha_q \rho_q \vec{v}_q) \right) = \sum_{p=1}^n (\dot{m}_{pq} - \dot{m}_{qp}) \quad (3)$$

where, ρ_{rq} is the phase reference density, or the volume averaged density of the q^{th} phase

in the solution domain, \vec{v}_q is the mean velocity of the q^{th} phase, \dot{m}_{pq} is the mass transfer

from phase p to phase q and \dot{m}_{qp} is the mass transfer from phase q to phase p .

Equation of Momentum for q^{th} Phase

$$\frac{\partial}{\partial t} (\alpha_q \rho_q \vec{v}_q) + \nabla \cdot (\alpha_q \rho_q \vec{v}_q \vec{v}_q) = -\alpha_q \nabla p + \nabla \cdot \underline{\underline{\tau}}_q + \alpha_q \rho_q \vec{g} + \sum_{p=1}^n (K_{pq} (\vec{v}_p - \vec{v}_q) + \dot{m}_{pq} \vec{v}_{pq} - \dot{m}_{qp} \vec{v}_{qp}) + (\vec{F}_q + \vec{F}_{lift,q} + \vec{F}_{wl,q} + \vec{F}_{vm,q} + \vec{F}_{td,q}) \quad (4)$$

where, \vec{g} is the acceleration due to gravity, $\underline{\underline{\tau}}_q$ is the q^{th} phase stress-tensor, \vec{F}_q is an external body force, $\vec{F}_{lift,q}$ is a lift force, $\vec{F}_{wl,q}$ is a wall lubrication force, $\vec{F}_{vm,q}$ is a virtual mass force, $\vec{F}_{td,q}$ is a turbulent dispersion force, p is the pressure shared by all phases, \vec{v}_{pq} and \vec{v}_{qp} are the interphase velocities and K_{pq} is the interphase momentum exchange coefficient.

$k - \varepsilon$ Turbulence Model for q^{th} Phase

$$\begin{aligned} \frac{\partial}{\partial t} (\alpha_q \rho_q k_q) + \nabla \cdot (\alpha_q \rho_q \vec{U}_q k_q) &= \nabla \cdot \left[\alpha_q \left[\mu_q + \frac{\mu_{t,q}}{\sigma_k} \right] \nabla k_q \right] \\ &+ (\alpha_q G_{k,q} - \alpha_q \rho_q \varepsilon_q) + \sum_{p=1}^N K_{pq} (c_{pq} k_p - c_{qp} k_q) \\ &- \sum_{p=1}^N K_{pq} (\vec{U}_p - \vec{U}_q) \frac{\mu_{t,p}}{\alpha_p \sigma_p} \nabla \alpha_p \\ &+ \sum_{p=1}^N K_{pq} (\vec{U}_p - \vec{U}_q) \frac{\mu_{t,q}}{\alpha_q \sigma_q} \nabla \alpha_q + \Pi_{k_q} \end{aligned} \quad (5)$$

$$\begin{aligned} \frac{\partial}{\partial t} (\alpha_q \rho_q \varepsilon_q) + \nabla \cdot (\alpha_q \rho_q \vec{U}_q \varepsilon_q) &= \nabla \cdot \left[\alpha_q \left[\mu_q + \frac{\mu_{t,q}}{\sigma_\varepsilon} \right] \nabla \varepsilon_q \right] + \frac{\varepsilon_q}{k_q} [C_{1\varepsilon} \alpha_q G_{k,q} \\ &- C_{2\varepsilon} \alpha_q \rho_q \varepsilon_q + C_{3\varepsilon} \left(\sum_{p=1}^N K_{pq} (c_{pq} k_p - c_{qp} k_q) \right. \\ &- \sum_{p=1}^N K_{pq} (\vec{U}_p - \vec{U}_q) \frac{\mu_{t,p}}{\alpha_p \sigma_p} \nabla \alpha_p \\ &\left. + \sum_{p=1}^N K_{pq} (\vec{U}_p - \vec{U}_q) \frac{\mu_{t,q}}{\alpha_q \sigma_q} \nabla \alpha_q \right)] + \Pi_{\varepsilon_q} \end{aligned} \quad (6)$$

where, k_q is the turbulent kinetic energy of the q^{th} phase, ε_q is the eddy dissipation of the q^{th} phase, \vec{U}_q and \vec{U}_p are the phase weighted velocities, μ_q is the molecular viscosity of the q^{th} phase, $\mu_{t,p}$ and $\mu_{t,q}$ are the turbulent viscosities in terms of turbulent kinetic energy of p^{th} and q^{th} phase, $G_{k,q}$ is the production of turbulent kinetic energy, Π_{k_q} and Π_{ε_q} are the source terms, c_{pq} and c_{qp} are approximated as $c_{pq} = 2$, $c_{qp} = 2 \left(\frac{\eta_{pq}}{1 + \eta_{pq}} \right)$, η_{pq} is the ratio between the two characteristic times and σ_k , σ_q , σ_p , $C_{1\varepsilon}$, $C_{2\varepsilon}$, $C_{3\varepsilon}$ are the model constants.

8. Solver Settings

The problem of vehicle external flow numerical analysis requires the solver settings to be completed before starting the simulations. The solver setting includes type of solver (3D or 2D), the viscous model, boundary conditions and solution controls. The inlet of the wind tunnel was indicated by the term “velocity-inlet”, while the outlet of the wind tunnel was termed as “pressure-outlet”. The solver settings used for the present simulations are shown in the tables below table 5.

Table 5. Solver setting used for the present simulations

Solver	Pressure- Based
Time	Transient
Model	Multi-phase
Primary Phase	Air
Secondary Phase	Sand-Dust up
Phase Interactions	Wen-Yu Mode
Viscous Model	K-Epsilon
K-Epsilon Model	Realizable
Near- Wall Treatment	Non-Equilibri
Turbulence Multiphase Model	Per Phase

9. Discussion of Results

The results from simulations in dusty-fluid 2D Ahmed body simulations as presented and discussed in this section. The pressure contour plot at the Ahmed body's symmetry plane reveals that the Ahmed body's front nose suffers increased pressure as the total kinetic energy is converted to pressure energy (Stagnation Point). Additionally, as the volume fractions of dusty fluid increases to 0.1 percent, the total pressure increases as well, as shown in Figure 4.

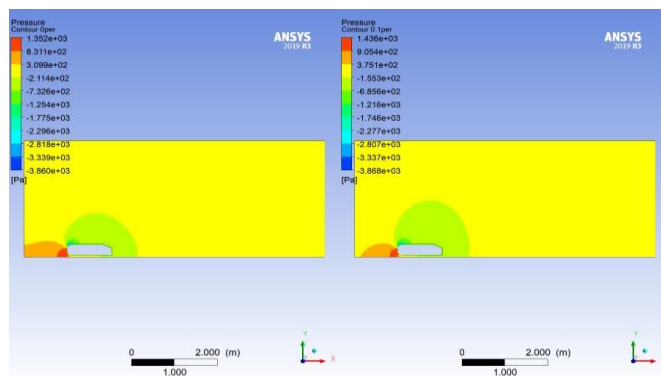


Figure 4. Pressure contour plots comparison at 0 and 0.1% volume fractions of suspended dust particles.

The picture 5 illustrates the velocity contour plots at the symmetry plane of the Ahmed body. As can be seen from the figure, it follows the Bernoulli principle and is therefore the inverse of the pressure contour. As the concentration of suspended dust particles in the air increases, the maximum velocity increases to 88.12 m/s at 0.1 percent. This is because the suspended dust attempts to dampen the air velocity, so reducing the flow.

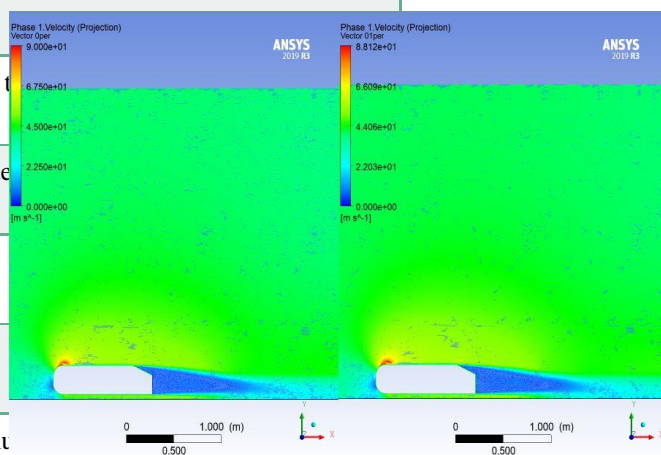


Figure 5. Velocity contour plots comparison at 0 and 0.1% volume fractions of suspended dust particles.

Figure 6 depicts the flow structures in the Ahmed body's rear portion. As previously indicated, the flow splits at the top edge's centre area and reattaches on the slant for the rear slant angle of 25° (Guilmineau, 2008). When suspended dusty fluid flows are evaluated at both intensity levels, similar flow topologies are predicted. Additionally, the wake generates two anticlockwise eddies with identical generating regions.

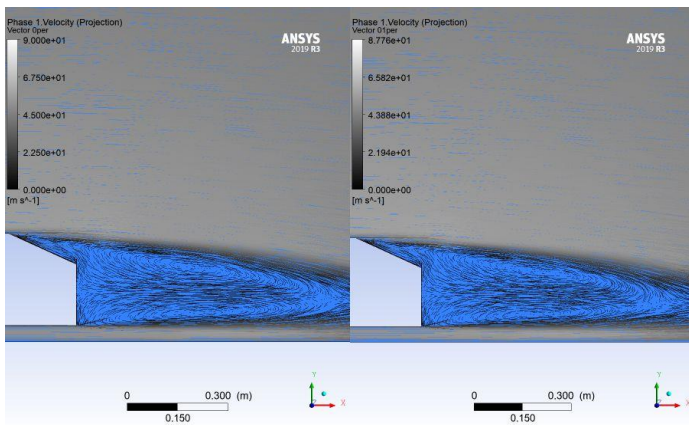


Figure 6. Velocity wakes contour plots comparison at 0 and 0.1% volume fractions of suspended dust particles.

Figure 7 illustrates the Drag Coefficients found and their comparison to earlier experimental (ERCOFTAC) and single phase simulation results. As seen in the bar chart, the simulation using the dusty fluid model accurately predicts the drag coefficient. The accumulated total drag coefficient for suspended dust particles in air at a volume fraction of 0.1% is around 0.292. Additionally, the relative error determined from the drag coefficients is shown in Table 6.

Table 6. Relative error comparison for drag coefficient values

Experimental , Cd (A)	Simulations, Cd (B)	Two- Phase Simulations, Cd (C)	Relative Error (%) Between (B) & (C)	Relative Error (%) Between (A) & (C)
0.283 (S. R. Ahmed, 1984)	0.31 (Khan and Umale, 2014)	0.292	5.80	3.18

With a 0.1% volume fraction increase in suspended dust particles in air, it is observed that the highest relative error when compared to the existing experimental result is approximately 3.18 percent, however it is approximately 5.80 percent when compared to the simulation findings. This demonstrates that the presence of dust suspended particles in the air has an effect on the aerodynamics flow characteristics, hence decreasing the overall drag coefficient regardless of the system's body shape.

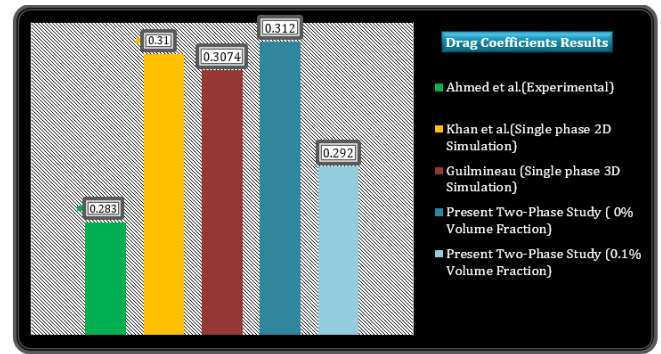


Figure 7. Drag Coefficients comparison of dusty-fluid simulations with existing results

10. Conclusion

The drag performance and overall flow characteristics in the presence of a dusty fluid environment have been investigated utilizing the k-epsilon turbulence scheme in a 2D 25° rear slant Ahmed body. The conclusions are highlighted herewith.

- i. As suspended dust volume fractions increases to 0.1 percent, the total pressure over the Ahmed body also get increase.
- ii. A similar flow topology has been achieved in presence of suspended dust at 0.1 percent volume fractions, i.e. the flow gets separated from the top edge of the rear slant and gets reattachment towards the mid of the slant surface of the Ahmed body.
- iii. The maximum relative error in overall drag coefficient values in presence of suspended dust particle volume fractions in air by 0.1 percent is approximately 3.18 percent when compared to existing experimental data.
- iv. Turbulent flow simulations in dusty fluid medium produce a more accurate approximation to that of aerodynamic experimental wind tunnel results as compared to single-phase turbulent simulations, signifying a more effective approach for such investigations.

References

1. Aljure, D. E. et al. (2014) 'Computers & Fluids Flow and turbulent structures around simplified car models', *COMPUTERS AND FLUIDS*. Elsevier Ltd, 96, pp. 122–135. doi: 10.1016/j.compfluid.2014.03.013.
2. Ashton, N. et al. (2016) 'Assessment of RANS and DES methods for realistic automotive models', *Computers and Fluids*. Elsevier Ltd, 128, pp. 1–15. doi: 10.1016/j.compfluid.2016.01.008.
3. Fares, E. (2006) 'Unsteady flow simulation of the Ahmed reference body using a lattice Boltzmann approach', *Computers and Fluids*, 35(8–9), pp. 940–950. doi: 10.1016/j.compfluid.2005.04.011.
4. Fluent 6.3.26 users guide (2015), <https://www.Fluent.com>.
5. Gaylard, A. P. et al. (2017) 'Simulation of rear surface contamination for a simple bluff body', *Journal of Wind Engineering and Industrial Aerodynamics*. Elsevier Ltd, 165(February), pp. 13–22. doi: 10.1016/j.jweia.2017.02.019.
6. http://www.ercsoftac.org/fileadmin/user_upload/bigfiles/sig15/data_base/index.html.
7. Le Good, G. M. and Garry, K. P. (2004) 'On the use of reference models in automotive aerodynamics', *SAE Technical Papers*, 2004(724). doi: 10.4271/2004-01-1308.
8. Guilmineau, E. (2008) 'Computational study of flow around a simplified car body', *Journal of Wind Engineering and Industrial Aerodynamics*, 96(6–7), pp. 1207–1217. doi: 10.1016/j.jweia.2007.06.041.
9. Guilmineau, E., Queutey, P. and Visonneau, M. (2018) 'Assessment of Hybrid LES Formulations for Flow Simulation Around the Ahmed Body', *Computers and Fluids*. Elsevier Ltd, (January). doi: 10.1016/j.compfluid.2017.01.005.
10. Khan, R. S. and Umale, S. (2014) 'CFD Aerodynamic Analysis of Ahmed Body', 18(7), pp. 301–308.
11. Lienhart, H. and Becker, S. (2003) 'Flow and turbulence structure in the wake of a simplified car model', *SAE Technical Papers*, pp. 323–330. doi: 10.4271/2003-01-0656.
12. Mishra, S. et al. (2019) 'MULTIPHASE MIXTURE MODEL SIMULATION OVER A SIMPLIFIED CAR', 23(1), pp. 17–24.
13. Morgut, M. and Nobile, E. (2012) 'Influence of grid type and turbulence model on the numerical prediction of the flow around marine propellers working in uniform inflow', *Ocean Engineering*. Elsevier, 42, pp. 26–34. doi: 10.1016/j.oceaneng.2012.01.012.
14. Pandey, M., Padhi, B. N. and Mishra, I. (2021) 'Performance analysis of a waste heat recovery solar chimney for nocturnal use', *Engineering Science and Technology, an International Journal*. Karabuk University, 24(1), pp. 1–10. doi: 10.1016/j.jestch.2020.11.009.
15. Mishra, S., Misra, A., Rao, P. S. V. R., Rao, D. N., (2017). Simulation of Aerodynamic Flow Parameters over a Simplified Sedan Car. *International Journal of Engineering, Science and Mathematics*, 6(8), 1265-1274.
16. S. R. Ahmed, G. R. and G. F. (1984) 'Some Salient Features of the Time -Averaged Ground', 93, pp. 473–503.
17. Serre, E. et al. (2013) 'Computers & Fluids On simulating the turbulent flow around the Ahmed body: A French – German collaborative evaluation of LES and DES', *Computers and Fluids*. Elsevier Ltd, 78, pp. 10–23. doi: 10.1016/j.compfluid.2011.05.017.
18. Tientcheu-Nsiewe, M. et al. (2016) 'Ahmed body, Wake, Velocity field, Turbulent flow, CFD; Ahmed body, Wake, Velocity field, Turbulent flow, CFD', *American Journal of Environmental Engineering*, 6(6), pp. 157–163. doi: 10.5923/j.ajee.20160606.01.